# Pseudo-Doherty Load-Modulated Balanced Amplifier With Wide Bandwidth and Extended Power Back-Off Range

Yuchen Cao<sup>®</sup>, Student Member, IEEE, and Kenle Chen<sup>®</sup>, Member, IEEE

Abstract-This article presents a novel architecture of load-modulated balanced amplifier (LMBA) with a unique load-modulation characteristic different from any existing LMBAs and Doherty power amplifiers (DPAs), which is named pseudo-Doherty LMBA (PD-LMBA). Based on a special combination of control amplifier (carrier) and balanced amplifier (peaking) together with proper phase and amplitude controls, an optimal load-modulation behavior can be achieved for PD-LMBA, leading to maximized efficiency over extended power back-off range. More importantly, the efficiency optimization can be achieved with only a static setting of phase offset at a given frequency, which greatly simplifies the complexity for phase control. Furthermore, the cooperations of the carrier and peaking amplifiers in PD-LMBA are fully decoupled, thus lifting the fundamental bandwidth barrier imposed on the Doherty-based active load modulation. Upon theoretical proof of these discoveries, a wideband RF-input PD-LMBA is physically developed using the GaN technology for experimental demonstration. The prototype achieves a highly efficient performance from 1.5 to 2.7 GHz, e.g., 58%-72% of efficiency at 42.5-dBm peak power and 47%-58% at 10-dB output back-off (OBO). When stimulated by a 10-MHz long term evolution (LTE) signal with a 9.5-dB peak-to-average power ratio (PAPR), the developed PD-LMBA achieves an efficiency of 44%-53% over the entire bandwidth at an average output power of around 33 dBm.

Index Terms—Balanced amplifier, Doherty, GaN, high efficiency, load modulation, power amplifier (PA), wideband.

#### I. INTRODUCTION

THE rapid evolution of wireless communications in the modern world has led to ever-increasing demands on higher data rates and lower system latency in communication links. Due to the scarcity of spectrum resources, the spectrum-efficient modulation schemes, such as high-order quadrature amplitude modulation (e.g., 1024QAM) and orthogonal frequency-division multiplexing (OFDM), have been widely exploited in cellular and wireless local area

Manuscript received October 28, 2019; revised January 10, 2020 and February 17, 2020; accepted February 21, 2020. Date of publication April 20, 2020; date of current version July 1, 2020. This work was supported by the National Science Foundation under Award 1914875. This article is an expanded version from the IEEE MTT-S International Microwave Symposium, Boston, MA, USA, June 2–7, 2019. (Corresponding author: Kenle Chen.)

The authors are with the Department of Electrical and Computer Engineering, University of Central Florida, Orlando, FL 32816 USA (e-mail: yuchencao@knights.ucf.edu; kenle.chen@ucf.edu).

Color versions of one or more of the figures in this article are available online at http://ieeexplore.ieee.org.

Digital Object Identifier 10.1109/TMTT.2020.2983925

network (WLAN) communications systems. Besides the benefits of those techniques, they have also led to a substantial increase of peak-to-average power ratio (PAPR) of signals, e.g., 7–8 dB in 4G versus >9.5 dB in 5G and WLAN IEEE 802.11ax [1], [2]. Amplification of such high-PAPR signals makes power amplifiers (PAs) suffer from substantial efficiency degradation. On the other hand, due to the communications band proliferation, the wireless spectrum has been significantly expanding toward higher frequencies beyond the conventional range from 0.7 to 2.7 GHz in the 2G-4G era. As a result, the operational bandwidth of a single PA is desired to be as wide as possible, in order to minimize the number of PAs on a wireless platform for reducing the cost, space, and system complexity.

Enhancement of PA efficiency primarily relies on two types of techniques, i.e., supply modulation (also known as envelope tracking) and load modulation. Given the bandwidth limitation and complexity in system operation of envelope tracking [3], load modulation has attracted increasing interest, and a variety of load-modulation architectures have been proposed and employed in realistic systems, including Doherty PA (DPA) [4]–[6], out-phasing PA [7]–[10], and varactor-based dynamic load modulation [11]-[15]. However, conventional load-modulation techniques are facing difficulties in efficiently transmitting the high-PAPR signals and in extending to wider bandwidth. For example, the standard DPA only offers 6 dB of back-off power range, while the bandwidth is strongly limited by the quarter-wave inverter embedded in its circuit schematic. Despite recent advances in terms of wideband asymmetrical DPAs [16]-[18], distributed DPAs [19], [20], and multiway DPAs [21], [22], maintaining maximized efficiency over extended power back-off and meanwhile over broadened frequency span still remains a major challenge. Therefore, to enable energy-efficient and wideband communications for future generations, there is an urgent demand to discover a new type of load-modulation PA fundamentally breaking the efficiency-bandwidth compromise.

Recently, a new PA architecture, load-modulated balanced amplifier (LMBA), has been demonstrated exhibiting an effective method for performing load modulation over wide bandwidth [23]–[28]. By injecting an external signal into the isolation port of the output quadrature coupler, the load impedances of balanced amplifier (BA) devices can be controlled with the variation of this signal's amplitude

0018-9480 © 2020 IEEE. Personal use is permitted, but republication/redistribution requires IEEE permission. See https://www.ieee.org/publications/rights/index.html for more information.

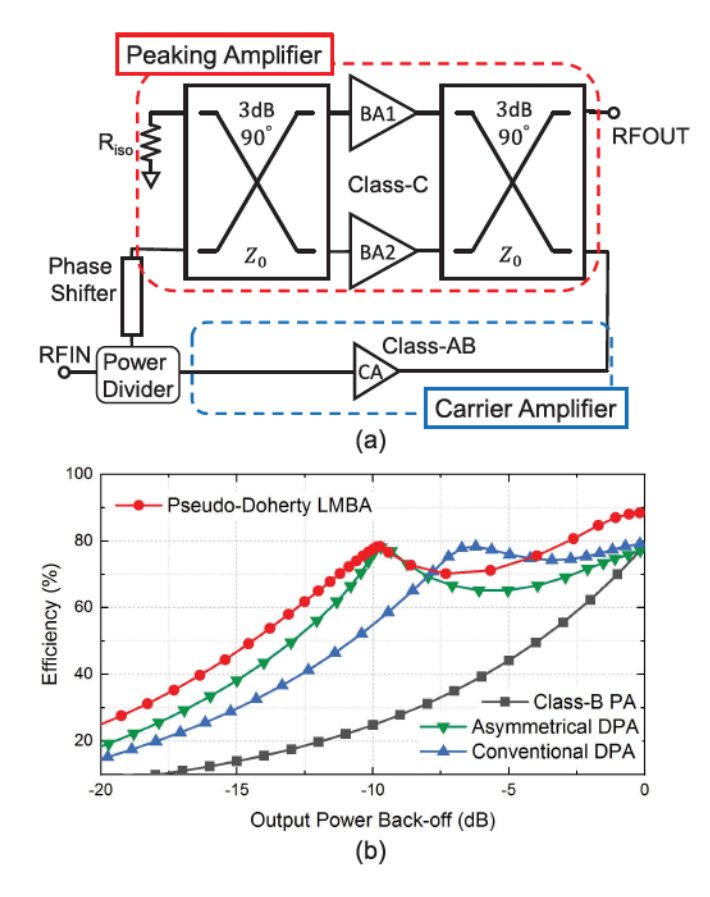


Fig. 1. PD-LMBA overview. (a) Schematic and (b) simulated efficiency profile comparison between Class-B amplifier, conventional DPA, asymmetrical DPA, and PD-LMBA (simulation is based on bare-die GaN devices to emulate the ideal transistor models).

and phase, leading to the load-modulation behavior and enhanced back-off efficiency. Moreover, by introducing a control amplifier (CA) generating the control signal and by merging its input with BA, the single-input (or RF-input) LMBA is formed [24], [29]. The LMBA can be further incorporated with Doherty-like combination of BA (carrier) and CA (peaking), leading to Doherty-like load-modulation behavior [30]. However, it is noted that the power back-off range is not fully expanded beyond the 6-dB range for the existing LMBA designs [25], [28], while the back-off efficiency optimization relies on concurrent amplitude and phase controls [25], [28], [31]. Such a control scheme requires dynamic phase tuning that could increase the system-level complexity.

Based on the classic LMBA theory [23] and the Doherty-like RF-input LMBA method [24], [25], this article redesigns the LMBA architecture, as shown in Fig. 1(a). By setting the BA as the peaking and CA as the carrier, a unique Doherty-like LMBA mode is discovered different from any existing LMBAs and DPAs, which is named pseudo-Doherty LMBA (PD-LMBA). It is for the first time revealed that the operations of BA and CA in this redefined LMBA are functionally independent and decoupled. This unprecedented load-modulation mechanism circumvents the difficulties in wideband implementation of active load modulations, e.g., Doherty or out phasing, which are all based on coupled interaction between

multiple amplifiers. Moreover, with proper settings of BA–CA power scaling ratio and phase offset, the power back-off range of PD-LMBA can be greatly extended beyond the 6 dB of conventional DPA [32], [33] without compensating the back-off efficiency such as asymmetrical DPA [16], [17], as shown in Fig. 1(b). Meanwhile, it is important to emphasize that at a given frequency, the optimized back-off efficiency can be achieved with only a static setting of phase offset, and the wideband phase shifting between BA and CA can be easily implemented using a transmission line (TL). These features minimize the circuit and system complexity. Based on the established PD-LMBA theory, a prototype is physically developed and experimentally demonstrated, exhibiting the state-of-the-art performance in terms of bandwidth, power back-off range, and efficiency. In order to comprehensively exhibit the PD-LMBA theory, it will be analyzed in detail in Section II with analytical derivation, which will be further validated by practical design in Section III and experimental demonstration in Section V. The consistency between theory, ideal-model simulation [see Fig. 1(b)], and practical design proves that the PD-LMBA theory can be generalized to any design based on this architecture.

#### II. ADVANCED PSEUDO-DOHERTY LMBA THEORY

Based on the recently reported LMBA theory [23], a new LMBA mode is proposed in conjunction with a novel Doherty-like cooperation of CA (main) and balanced amplifier (peaking), which leads to an optimized load-modulation behavior if the proper amplitude and phase controls are performed. With such a unique pseudo-Doherty load-modulation characteristic, this new type of LMBA is theoretically analyzed in this section.

# A. Review of LMBA

The LMBA described in [23] is derived from a convectional BA architecture [34] with two amplifiers combined in  $90^{\circ}$  out-of-phase using two classical quadrature hybrids at input and output. The LMBA differs from a standard BA in circuitry that the isolation port of the output coupler is not terminated to a resistor of characteristic impedance,  $Z_0$ , while a control signal is injected therein instead. With two symmetrical balanced amplifiers (BA1 and BA2) and the control signal, the behavior of LMBA can be considered as three excitation sources driving the output quadrature coupler, and it can be analytically described using the impedance matrix given by

$$\begin{bmatrix} V_1 \\ V_2 \\ V_3 \\ V_4 \end{bmatrix} = Z_0 \begin{bmatrix} 0 & 0 & +j & -j\sqrt{2} \\ 0 & 0 & -j\sqrt{2} & +j \\ +j & -j\sqrt{2} & 0 & 0 \\ -j\sqrt{2} & +j & 0 & 0 \end{bmatrix} \begin{bmatrix} I_1 \\ I_2 \\ I_3 \\ I_4 \end{bmatrix}$$
(1)

where  $I_2 = I_b$  and  $I_4 = -jI_b$  represent the input currents from BA1 and BA2 and  $I_3 = jI_ce^{j\theta}$  denotes the current from control signal source [23], as shown in Fig. 1(a).

Qualitatively speaking, due to the symmetry of quadrature coupler, the injected control signal is split equally into two halves appearing at the drain of the PA of each branch, which interacts with the output signals generated by these two

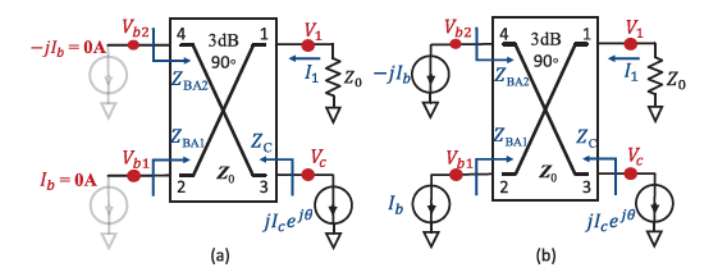


Fig. 2. Ideal generalized schematic of the output combining network for analyzing the proposed PD-LMBA architecture. (a)  $P_{\rm OUT} < P_{\rm Max}/{\rm OBO}$ . (b)  $P_{\rm OUT} \ge P_{\rm Max}/{\rm OBO}$ .

branch PAs leading to load-modulation behavior. Using the matrix operation illustrated in (1), the impedances of BA1 and BA2 can be calculated as

$$Z_{BA1} = Z_{BA2} = Z_0 \left( 1 + \frac{\sqrt{2}I_c e^{j\theta}}{I_b} \right)$$
 (2)

where  $I_b$  is the magnitude of BA currents,  $I_c$  is the magnitude of CA current, and  $\theta$  is the phase of the control path [23].

While the original LMBA requires dual inputs, the single input (or RF-input) LMBA has been proposed and demonstrated [24], [29]. The RF-input LMBA uses a CA instead of an independent control signal power (CSP). The CA shares the same RF input with the BA, and the input power is split into BA and CA at a given ratio through a dedicated power divider. The CA supplies control power into the isolation port of the output coupler. The load impedance of BAs is dependent on both the power (i.e., current) and the phase of the control signal generated by CA. The operation of LMBA is primarily dependent on the following two aspects: 1) amplitude control of CA, which can be designed with proper power dividing ratio at the RF input node and the peak power ratio between BA and CA and 2) phase control of CA, which can be realized through a properly defined static phase offset,  $\theta_0$  [29], and a dynamically tunable phase  $\Delta\theta$  [31].

## B. Pseudo-Doherty LMBA Mode

In the RF-input Doherty-like LMBA described in [30], the BA is biased to Class-AB acting as the carrier amplifier, and the CA is biased to Class-C as the peaking amplifier. This cooperation of BA and CA exhibits a standard Doherty-like behavior with load modulation from peak power to 6-dB back-off. In this design, the carrier-peaking combination of BA and CA is swapped targeting for an extended range of output back-off (OBO), e.g., up to 10 dB, and enhanced back-off efficiency. To theoretically analyze the PD-LMBA, its operation is divided into the following three regions.

1) Low-Power Region ( $P_{OUT} < P_{Max}/OBO$ ): When the PA is operating at low power level below the predefined target OBO power, the BA is completely turned off, i.e.,  $I_b = 0$ , as shown in Fig. 2(a). In this case, the output power is only generated by the CA. According to (2), the impedances of BA1 and BA2 are thus equal to  $\infty$ ; a further derivation using the matrix operation in (1)

indicates a CA impedance of Z<sub>0</sub>

$$Z_{\text{BA1,LP}} = Z_{\text{BA2,LP}} = \infty$$

$$Z_{\text{C,LP}} = Z_0. \tag{3}$$

In this region, the overall LMBA efficiency is equal to the efficiency of CA, which increases toward maximum as the CA power saturates at the target OBO power.

2) Back-Off Region ( $P_{\text{Max}}/\text{OBO} \leq P_{\text{OUT}} < P_{\text{Max}}$ ): Once the power is increased to the target OBO level, the CA should reach to its saturation, leading to  $I_c = I_{c,\text{Max}}$ . As the power further increases, the BA is turned on and  $I_b$  starts to increase from 0 toward  $I_{b,\text{Max}}$ , as shown in Fig. 2(b). Since the loading of CA remains to be  $Z_0$  as calculated using (1), the saturation of CA is maintained, while  $I_c$  remains its maximum value of  $I_{c,\text{Max}}$ . In this back-off region, the load-modulation behavior of BA1 and BA2 as well as the CA impedance are given by

$$Z_{\text{BA1,BO}} = Z_{\text{BA2,BO}} = Z_0 \left( 1 + \frac{\sqrt{2}I_{c,\text{Max}}e^{j\theta}}{I_b} \right)$$

$$Z_{\text{C,BO}} = Z_0. \tag{4}$$

In this region, the CA remains saturated with the highest efficiency, while BA's efficiency can also be significantly boosted through load modulation. As a result, an enhanced back-off efficiency of the overall LMBA can be achieved.

3) Saturation Region (P<sub>OUT</sub> = P<sub>Max</sub>): As the power increases to the saturation of BA, the CA and BA are saturated simultaneously. In this condition, the saturation load impedances of BA1, BA2, and CA are as follows:

$$Z_{\text{BA1,SAT}} = Z_{\text{BA2,SAT}} = Z_0 \left( 1 + \frac{\sqrt{2} I_{c,\text{Max}} e^{j\theta}}{I_{b,\text{Max}}} \right)$$
$$Z_{\text{C,SAT}} = Z_0. \tag{5}$$

The ratio of  $I_{c,\text{Max}}/I_{b,\text{Max}}$  is dependent on the OBO range, and this ratio becomes smaller as OBO increases. At this saturation region, the entire LMBA achieves the maximum efficiency.

It is important to note that the loading of CA is constantly  $Z_0$  across all three regions. In comparison with Doherty PA, this unique feature eliminates the necessity of impedance inverter connected to the main amplifier, fundamentally breaking the bandwidth limitation imposed on the Doherty PA. Meanwhile, unlike the main amplifier in the Doherty PA, the load impedance of CA is not affected by the OFF-state impedance of the peaking amplifier (i.e., BA), leading to significantly reduced complexity for a wideband design [35], [36]. Compared to the sequential amplifier with no load modulation that compromises PA efficiency at  $P_{\text{Max}}$  [18], [37], [38], PD-LMBA realizes the BA load modulation through a special combination of BA and CA, which maintains a high-efficiency throughout  $P_{\text{Max}}$  and the target OBO. The overall operation of PD-LMBA primarily relies on the amplitude and phase control of the main balanced amplifier through the CA, which is discussed in detail in Sections III and IV.

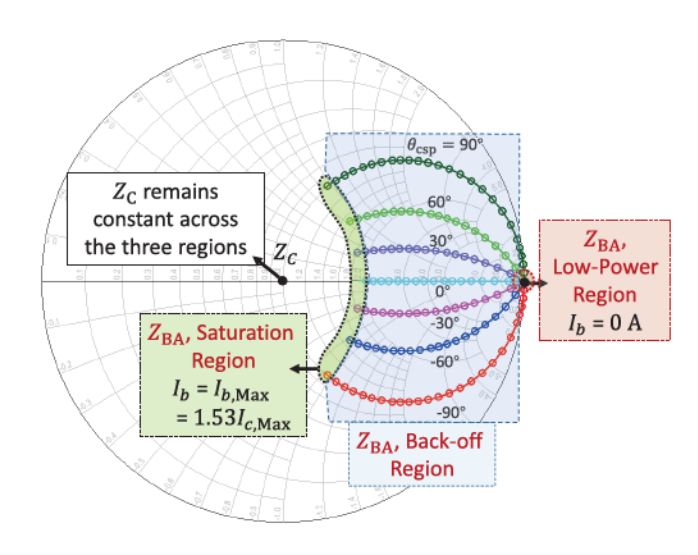


Fig. 3. Dynamic BA and CA load impedances using the ideal generalized model (OBO = 10 dB).

# C. Amplitude Control of PD-LMBA

As indicated by (4), the amplitude control of PD-LMBA is mainly determined by the term of  $I_{c,\text{Max}}/I_b$ . In terms of the PD-LMBA operation, the BA needs to be turned on at the predetermined back-off power, where the CA reaches to its saturation simultaneously. Using the ideal model in Fig. 2, the current scaling ratio between CA and BA is determined by the target OBO range

$$\frac{1}{2}I_{c,\text{Max}}^{2} \times Z_{0} = \frac{\frac{1}{2}I_{c,\text{Max}}^{2} \times Z_{0} + 2 \times \left(\frac{1}{2}I_{b,\text{Max}}^{2} \times R_{\text{BA1,SAT}}\right)}{\text{OBO}}$$

$$I_{b,\text{Max}} = \frac{\sqrt{2 \times \text{OBO}} - \sqrt{2}}{2}I_{c,\text{Max}}.$$
(6)

In (6),  $R_{\rm BA1,SAT}$  is the real part of  $Z_{\rm BA1,SAT}$ . Practically, this BA–CA current scaling ratio can be transformed to the scaling ratio of transistor sizes of BA and CA. After determination of  $I_{c,{\rm Max}}/I_{b,{\rm Max}}$  according to a specific OBO (e.g.,  $I_{c,{\rm Max}}/I_{b,{\rm Max}}=1/1.53$  for 10 dB of OBO), the amplitude control of the load modulation is governed by the turn-on point of BA, which mainly depends on two factors: 1) the gate bias voltage of the BA  $V_{\rm GS,BA}$  and 2) the power dividing ratio between BA and CA. Both of these two factors will be considered together in the practical design.

# D. Phase Control of PD-LMBA

As indicated by (3)–(10), the balanced amplifier is equivalent to the peaking amplifier in the Doherty PA topology, in terms of the boundary points (e.g.,  $\infty$  and  $Z_0$ ) of the corresponding load-modulation trajectory. Meanwhile, the trajectory connecting these two boundary points is solely determined by the phase of the CSP, i.e.,  $\theta = \theta_{\rm csp}$ , given the fixed  $I_{c,{\rm Max}}/I_{b,{\rm Max}}$  ratio determined using (6) with a specific target OBO. Fig. 3 shows the load trajectory of BA with a variation of  $\theta_{\rm csp}$  for OBO of 10 dB. Unlike the asymmetrical Doherty PAs [16], [17], [39], [40], the load modulation of BA, as the peaking amplifier of PD-LMBA, can be maintained

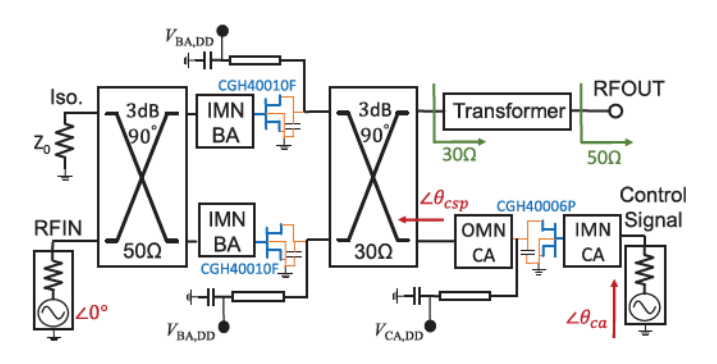


Fig. 4. Simulation setup of the proposed PD-LMBA using realistic GaN transistors for analysis and verification.

along the real axis by setting  $\theta_{csp}$  to 0°. It is important to emphasize that this constantly resistive load trajectory is the optimal solution as explained by the classical Class-B loadline theory [38]. Such a load-modulation behavior ideally ensures a maximized back-off efficiency of the PD-LMBA, which can be considered the major advantage over asymmetrical Doherty PA for extension of dynamic power range. It is also surmized that there is no need to dynamically change the phase of CA as a function of power, which has been necessary in other reported LMBAs [23], [41], [42]. This unique characteristic is highly desired for RF-input LMBA designs, in which the dynamic phase control is difficult compared with the dual-input LMBA design.

In summary, the PD-LMBA architecture proposed in this article primarily has four advantages over the other reported LMBAs and other load-modulation techniques.

- The power asymmetry between carrier and peaking amplifiers can be easily realized for achieving extended power back-off range since the BA with two PAs combined is naturally stronger in power generation than the single branch of CA.
- 2) As the carrier amplifier, CA is loaded with a constant impedance ideally not affected by the OFF-state impedances of BA1 and BA2, which significantly simplifies the complexity of broadband design without having to control the load trajectory of the carrier amplifier over a wide frequency range.
- The cooperation of BA and CA in PD-LMBA ensures an optimized load-modulation trajectory of the BA, leading to the maximized efficiency over the entire extended power back-off range.
- 4) At any given in-band frequency, the optimal load-modulation behavior can be achieved only by setting a static phase offset between BA and CA, thus minimizing the circuit and system complexity.

# III. PRACTICAL DESIGN OF PD-LMBA FOR OPTIMIZED EFFICIENCY OVEREXTENDED POWER BACK-OFF RANGE

The PD-LMBA theory presented in Section II is based on ideal circuit components where the transistors are modeled as ideal current sources, while the effect of realistic components (e.g., parasitics of transistors) needs to be carefully considered

for implementation of the theory. This section focuses on the design of PD-LMBA using realistic circuit components, aiming at achieving the highest possible efficiency over extended dynamic power range (10 dB as targeted in this design).

Following the PD-LMBA theory and ideal schematic (see Fig. 2), a practical circuit of PD-LMBA is established using realistic GaN transistors, as the schematically shown in Fig. 4. Similar to the matching scheme presented in [42], the BA matching is realized through a combination of non-50- $\Omega$  quadrature coupler and bias line. This direct connection of transistor and coupler simplifies the load-modulation control of the realistic BAs [42] without being affected by excessive output matching networks. To better explain the PD-LMBA design in terms of amplitude control and phase control, the design starts with separated inputs of BA and CA, while these two independent sources will be replaced by a unified RF-input together with a power divider in the actual prototype development.

# A. Amplitude Control for Extended Power Back-Off Range

Based on the PD-LMBA operation described in Section II, the amplitude control consists of two essential parts: 1) determination of current/power scaling ratio between BA and CA and 2) saturation of CA (in Class-AB) and turn-on of BA (in Class-C) simultaneously at the target power back-off.

The maximum saturated power of CA is determined by the target OBO range and the overall maximum output power

$$P_{\text{CA,SAT}} = \frac{P_{\text{Total,SAT}}}{\text{OBO}} \tag{7}$$

where  $P_{\text{Total,SAT}}$  denotes the total maximum power generated by the entire LMBA, which combines the saturation power from BA and CA

$$P_{\text{Total,SAT}} = P_{\text{BA,SAT}} + P_{\text{CA,SAT}}.$$
 (8)

In this practical design with GaN transistors, the actual  $P_{\text{CA,SAT}}$  can be realized through proper selection of CA device size (6-W GaN transistor, Wolfspeed CGH40006P) and reduced drain bias voltage [31] for an extended OBO range of 10 dB. The maximum power of BA can be determined as

$$P_{\text{BA,SAT}} = (\text{OBO} - 1)P_{\text{CA,SAT}}.$$
 (9)

With the large target OBO, the high BA power can be achieved by using large-sized devices (10-W GaN transistor, Wolfspeed CGH40010F) together with full drain bias voltage and by combining the power of BA1 and BA2.

For the two variables governing the turn-on of BA, i.e., BA gate bias voltage and the input power dividing ratio, it is practically found that the effect of  $V_{\rm GS,BA}$  plays a dominant role. By setting the power dividing ratio between BA and CA to 1:1 (a ratio used in many reported RF-input LMBAs [24], [29]), the turn-on point of BA can be controlled solely through properly choosing the depth of Class-C bias. Fig. 5 shows the effect of BA turn-on point on the LMBA's efficiency versus power behavior. The highest power-added efficiency (PAE) over the entire power back-off range can be achieved only through the optimal turn-on setting of BA.

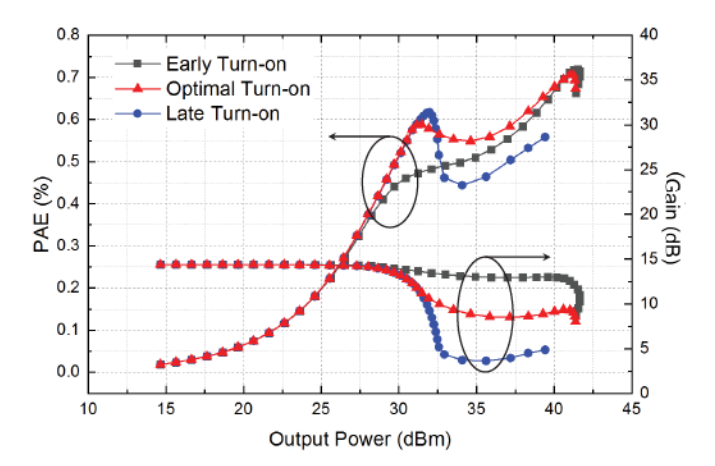


Fig. 5. Simulation results of PAE and gain verses output power at 2.3 GHz under different  $V_{\rm BA,GS}$  bias settings.

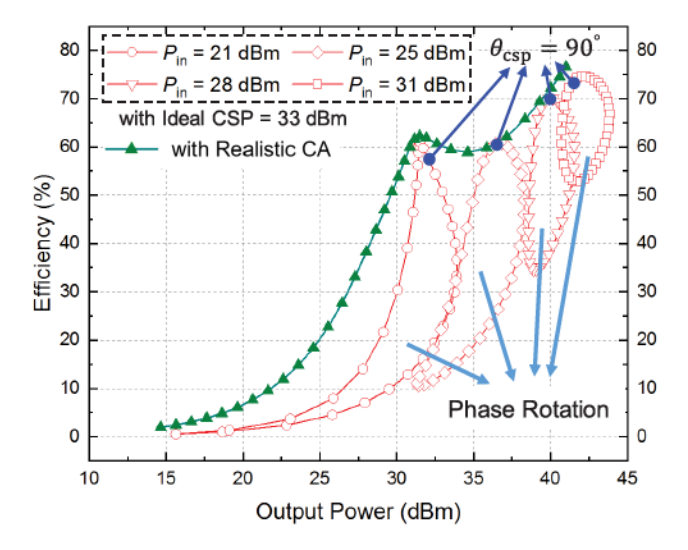


Fig. 6. Determination of the optimal phase offset based on the simulated large-signal performance at 2.3 GHz: using ideal CSP (= 33 dBm) with various phase settings versus using optimized CA ( $\theta_{ca} = -10^{\circ}$ ).

# B. Phase Control for Maximized Back-Off Efficiency

As discussed in Section II and shown in Fig. 3, there is an optimal phase setting of CA that leads to the optimal load-modulation trajectory and maximized efficiency. With the on-chip and package parasitics of realistic transistors, the optimal load trajectory of GaN devices in BA at the package plane must deviate from the ideal purely resistive load trajectory. Thus, a non-0° of control phase can be utilized to compensate for this effect. In order to find the optimal control phase, an ideal phase-swept RF source with constant CSP (= 33 dBm) is fed into the isolation port by replacing the actual CA. Assuming 70% of CSP efficiency, the overall LMBA efficiency is extracted with different BA input powers under 2 W of CSP through 360° phase rotation (10° of step size), as shown by the red curve in Fig. 6. It is important to point out that the highest efficiency points over the entire power back-off range correspond to a nearly constant control phase of  $\theta_{\rm csp} = 90^{\circ}$ , in comparison with the large variation of

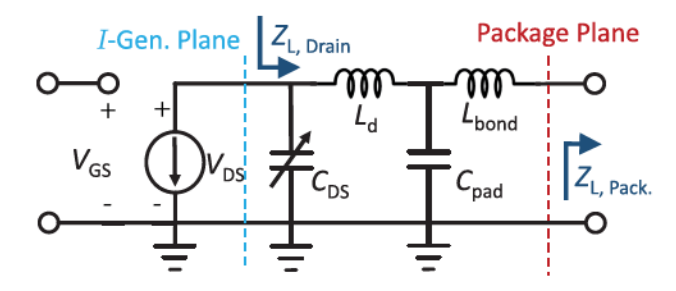


Fig. 7. Equivalent circuit model of CGH40010 showing the parasitics.

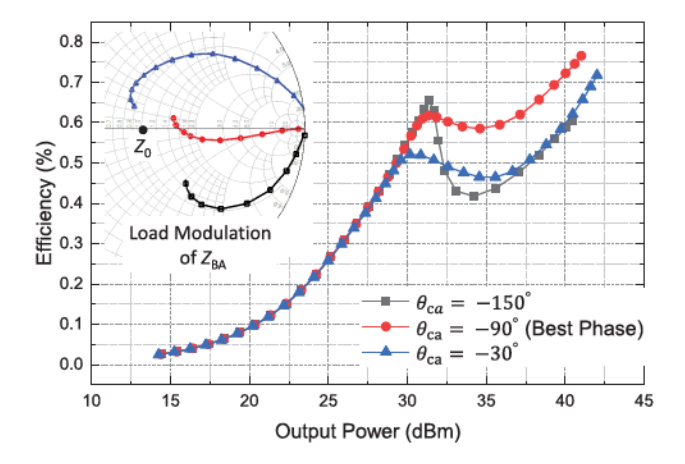


Fig. 8. Simulated efficiency profile at 2.3 GHz under different  $\theta_{ca}$  settings.

efficiency-optimal phase, as presented in [23] and [42]. The simulation results well verify the proposed PD-LMBA theory. Such an efficiency optimization with only static phase offset is not only applicable to the particular circuitry in Fig. 4, but it can also be expanded to all possible PD-LMBA circuit topologies.

With the realistic GaN-based CA connecting to the isolation port of the output quadrature coupler, the interface plane of phase control is moved from the isolation port to the input of CA, as shown in Fig. 4. By sweeping the input signal phase of CA, an optimal phase of  $\theta_{ca} = -10^{\circ}$  is obtained, which leads to maximized overall LMBA efficiency along the entire OBO range, as shown by the green curve in Fig. 6. The efficiency performance PD-LMBA design with realistic CA well matches the maximum efficiency achieved with ideal CSP. To fully verify the theory, the transistor parasitic network of BA is modeled (see Fig. 7) and deembedded to access the intrinsic drain load-modulation trajectory at the current generator plane, as shown in the inset Smith chart of Fig. 8. The intrinsic BA loadline tracks the resistive path from  $P_{\text{Max}}$ to 10-dB OBO, which well validates the theory. As the power level further decreases below 10-dB back-off, the BAs turns off and  $Z_{BA}$  approaches to the high-impedance region at the edge of Smith chart (see Fig. 8), while the power is primarily generated by CA only at this range.

# IV. WIDEBAND RF-INPUT PD-LMBA DESIGN

Based on the PD-LMBA theory and practical design presented in Sections II and III, it is interesting to note that the operations of BA and CA in the PD-LMBA are nearly independent because the CA's load impedance constantly remains  $Z_0$  and the BA's load modulation is mainly due to the variation of its own current ( $I_{c,\text{Max}}/I_b$  term in (4)). Given the fact that the individual BA and CA can both be expanded to wideband designs, the PD-LMBA exhibits promising wideband potential. Thus, the primary challenge for wideband PD-LMBA design shifts to the wideband phase control of CA to result in optimal load-modulation behavior of BA. Following the preliminary circuit schematic shown in Fig. 4, the wideband RF-input PD-LMBA design is performed by broadening the bandwidth of all the building blocks and by unifying the inputs of BA and CA to a single input with proper phase offset. In the prototype demonstration, the target bandwidth is from 1.5 to 2.7 GHz covering a majority of cellular communications bands.

# A. Wideband BA Design

The balanced amplifier comprises two identical PAs coupled in 90° out-of-phase through input and output quadrature couplers. The input coupler is built using a commercial device [43] with a wide operational bandwidth from 1 to 3 GHz. The output coupler is implemented using a three-section branch-line hybrid structure, which offers sufficient bandwidth covering the design target [44] and is codesigned with the PAs. The two balanced PAs are implemented with 10-W GaN transistors supplied by Wolfspeed [45](CGH40010F).

The PA output matching is performed using the non-50- $\Omega$ output coupler together with the bias line. From the load-pull simulation, the optimal load admittance  $(Y_L = G_L + j B_L)$  of the GaN transistor presents a nearly constant real part over the target frequency range, while the imaginary part increases (becoming less inductive) with frequency. Such a frequency response of the optimal loadline is mainly due to the parastics of the packaged GaN transistor, which has been observed in many wideband GaN PA designs [46]-[48]. Therefore, the characteristic impedance of the branch-line hybrid coupler,  $Z_1$ , is properly selected to provide the constant conductance  $(G_{\rm L}=1/Z_1)$  over the target bandwidth, and the bias line as a shunt inductor is utilized to provide the susceptance with the desired frequency response  $(jB_L = -j/(\omega L))$ . It is also noted that the BA's impedance in PD-LMBA at  $P_{BA,SAT}$  is different from the ideal BA with the contribution of CA, as indicated by (10). Therefore, the finalized value of  $Z_1$  (= 30  $\Omega$ ) and the bias-line length are determined through cosimulation with CA. A wideband 3:5 transformer follows a branch-line hybrid coupler to match the impedance to the 50- $\Omega$  terminal.

The input matching is designed and implemented using a multistage low-pass network based on TLs to cover the target bandwidth from 1.5 to 2.7 GHz. The design of such a matching circuit follows the well-established methodology presented in [46]. This article uses a four-section TL-based low-pass networks to realize the input matching, with each stage consisting of a series L (high-impedance TL) and shunt C (low-impedance open-ended stubs). The final lengths and widths of the TLs are tuned in order to absorb the parasitics of the RF and dc block as well as the device packaging.

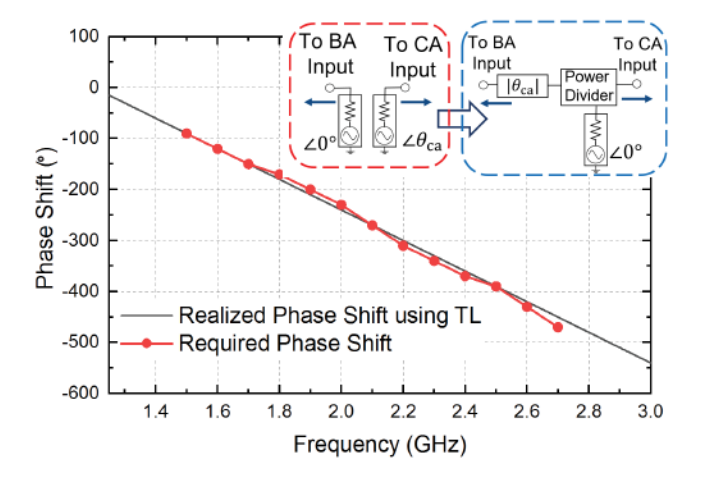


Fig. 9. Simulated optimal BA-CA phase offset at different frequencies and design of TL-based wideband phase shifter for merging the BA and CA inputs.

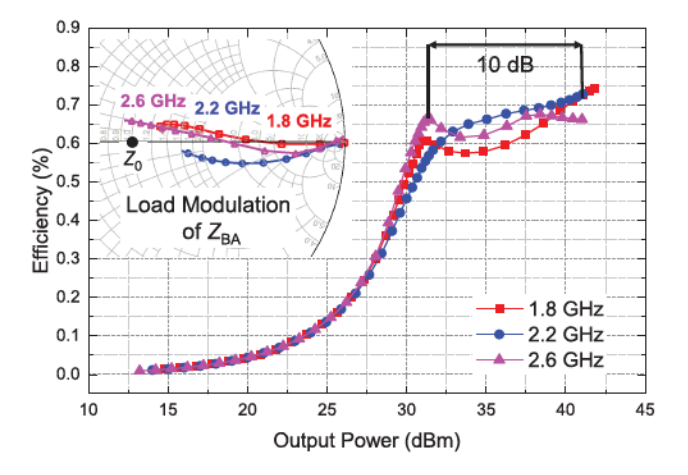


Fig. 10. Power-swept CW simulation results of the PD-LMBA for the best phase tuning setting at different frequencies.

# B. Wideband CA Design

According to the amplitude control scheme described in Sections II and III, the saturated power of CA determines the dynamic range once the BA power is fixed. To achieve the target OBO of 10 dB,  $P_{CA,SAT}$  should be around 9.5 dB below  $P_{\text{BA,SAT}}$ . To realize this low output power, the CA is implemented with a 6-W GaN transistor (Wolfspeed CGH40006P), and it is biased in the Class-AB mode with partial  $V_{\rm DD}$ . As the CA's maximum efficiency at  $P_{CA,SAT}$  determines the overall LMBA efficiency at the target OBO point, the design of CA as a single PA is aimed at achieving the highest possible efficiency. The output matching network design is performed to offer optimal loading impedance at both fundamental frequency and harmonics over the target bandwidth. Since the CA is directly connected to the non-50- $\Omega$  coupler, the design of output matching is based on the coupler characteristic impedance,  $Z_1$ .

For the input matching network design, we follow the same methodology in the BA's input design, and a three-section low-pass network based on TLs is designed to provide wideband input matching for the GaN transistor.

# C. Wideband BA-CA Phase Offset Design

Upon the completion of wideband BA and CA designs, the load modulation of BA is primarily governed by the relative phase between BA and CA. At a particular frequency, there is an optimal BA-CA phase offset that leads to the maximized back-off efficiency, as shown in Fig. 8. Using the dual-input (with equal amplitude) schematic in Fig. 4, the optimal phase offset is determined for each frequency point along the target bandwidth (0.1-GHz step), which is presented as the red dots in Fig. 9. It is noted that the optimal phase offset is almost linearly proportional to frequency with a negative slope. This frequency behavior can be easily implemented using a 50- $\Omega$  TL in connection with an in-phase input source, thus realizing a wideband phase shifter and offering accurate wideband phase control. Given the negative value of the relative phase between CA and BA, this offset TL in the CA path has a negative length, which can be physically

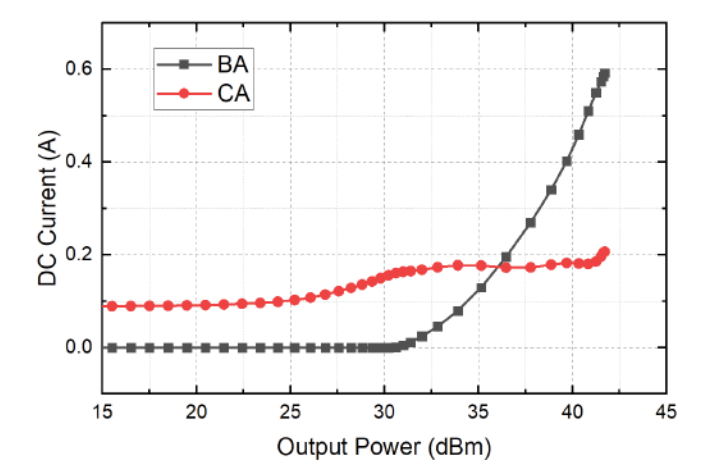


Fig. 11. Simulated drain dc current versus output power of BA (two BAs in total) and CA at 2.3 GHz.

implemented by placing a symmetrical TL with positive length in the BA path. With such a TL phase shifter, the dual inputs can be simply replaced by a single input with a standard wideband Wilkinson divider.

In the reported RF-input wideband LMBA designs [29], LC-based bandpass filter has been utilized to implement the BA-CA phase shifter for wideband phase control. However, the frequency response of the phase is very sensitive to the value of LC components. Given the unavoidable manufacturing variation in reality, it is difficult to accurately control all the component values in actual experiments, thus leading to a discrepancy between simulation and measurement. This sensitivity could also cause yield issues for massive production. The TL-based phase shifter well solves this problem and leads to minimized complexity for implementation.

The input power of the CA will continue to increase after reaching saturation at 10-dB OBO due to the RF-input, resulting in overdriving of the CA. It should be noted that the proposed architecture is mainly to maximize efficiency. The linearity is concerned as CA is overdriven, and the overdriving of the main amplifier has been utilized in another

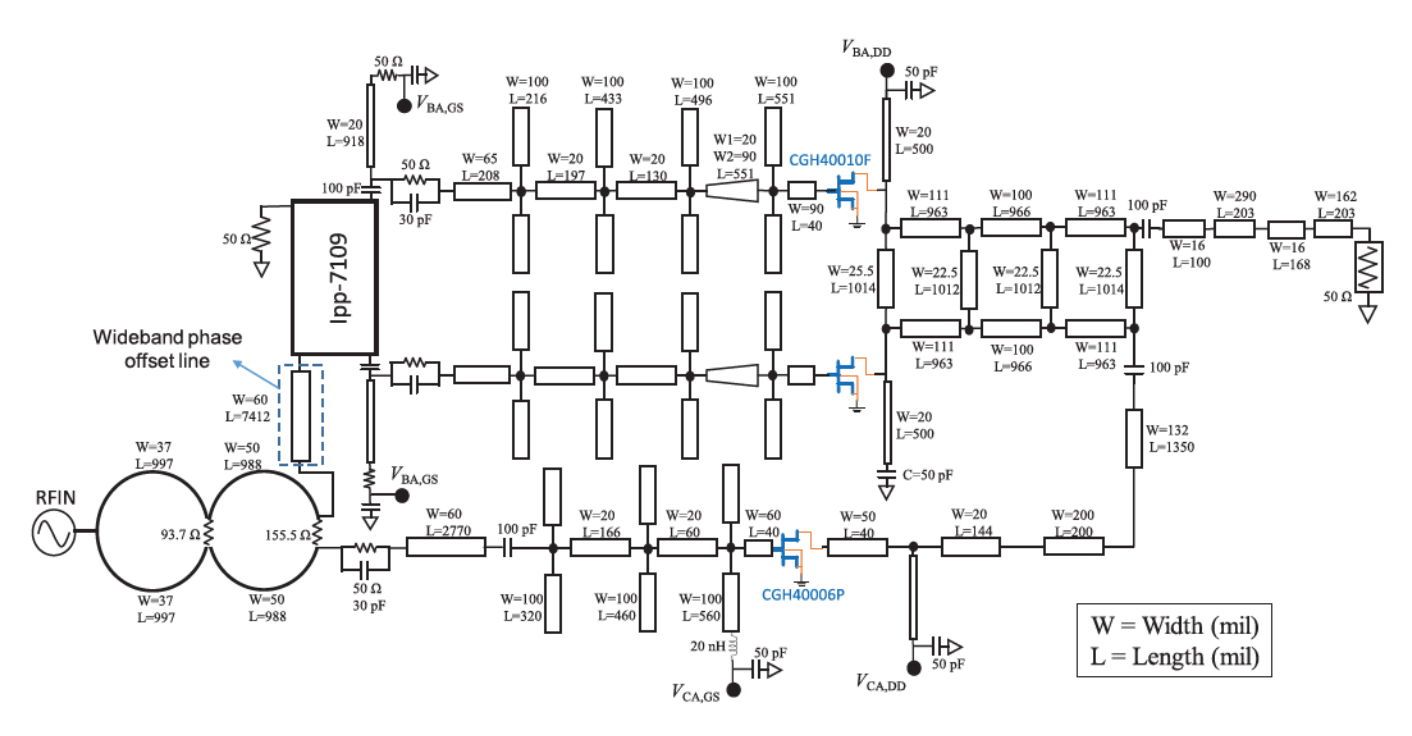


Fig. 12. Circuit schematic of designed PD-LMBA.

load-modulation architecture, i.e., DEPA, as presented in [20]. However, it has been demonstrated in [20] that such a behavior does not affect digital linearization performance.

# D. Overall Schematic and Simulation Results

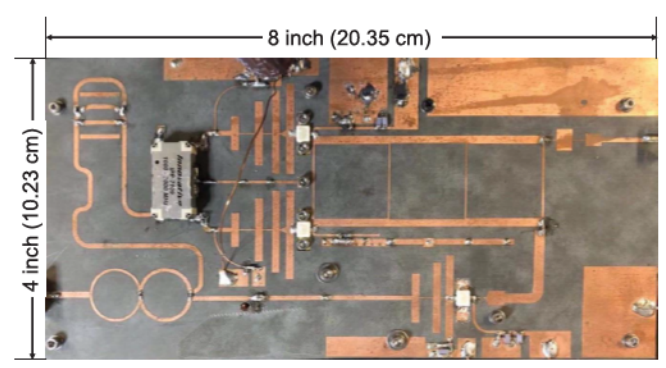
Through proper amplitude and phase control described in Sections IV-A-IV-C, the extended power back-off range and the optimal load-modulation trajectory can be achieved at different frequencies, as shown in Fig. 10. When the power falls below the target OBO, the output impedance of the BA transistor  $(Z_{BA})$  is close to the high-impedance region on the Smith chart edge. This means that the BA starts to turn off, while the power is purely generated by the CA. This Doherty-like behavior is achieved by properly setting the gate bias voltages of BA and CA below and above the transistor threshold, respectively. The dc current of BA and CA is extracted from the continuous-wave (CW) simulation to verify this PD-LMBA operation, as shown in Fig. 11. The turn-on point of BA is around 10-dB power back-off, where the CA approaches its saturation. As the power increases beyond 10-dB OBO, a strong peaking effect of BA current is observed in parallel with an almost stable CA current. Compared with the standard DPA's 6 dB load-modulation range, the PD-LMBA achieves more than doubled OBO range covering a wide frequency

Upon finishing the design of individual building blocks including BA, CA, and phase shifter, the integrated PD-LMBA circuit is built and the finalized circuit schematic of overview is shown in Fig. 12. The design values of all the circuit elements are exhibited alongside the schematic. The input power splitter is implemented using the two-stage Wilkinson divider for covering the target bandwidth. A wideband phase-offset TL is placed at the input port of BA. Moreover,

stabilizing circuits composing a parallel combo of capacitor and resistor are placed at the input of each individual amplifier. For this PD-LMBA architecture, the overall bandwidth is governed by the bandwidth of output coupler. In this design, the coupler is built with a multisection branch-line structure on a single-layer printed circuit board (PCB). It is difficult for this coupler structure to further increase the bandwidth, but a larger bandwidth can be achieved through advanced coupler designs based on multilayer PCB. Other than the input coupler that is a commercial off-the-shelf device (mainly for reducing the circuit footprint size), all the other individual building blocks, e.g., BA, CA, and output coupler, are not overdesigned in terms of bandwidth. The phase-offset line is added after optimizing the overall PD-LMBA using the dual-input model shown in Fig. 4. In practical PD-LMBA development, it should be optimized within the target bandwidth, and, ideally, the individual building blocks shall not be overdesigned.

# V. IMPLEMENTATION AND EXPERIMENTAL RESULTS

The designed broadband PD-LMBA prototype is fabricated on a 20-mil-thick Rogers Duroid-5880 PCB board with a dielectric constant of 2.2 and is mounted on a copper substrate for handling and measurement, as shown in Fig. 13. The PCB footprint size is 4 in  $\times$  8 in. The prototype is experimentally evaluated with both CW and modulated stimulation signals. In the measurement, the BA is biased in Class-C with 28 V of  $V_{\rm DS,BA}$ . The gate bias voltage  $V_{\rm GS,BA}$  is set between -5 and -4 V to obtain the best PAE in the test, which varies with different frequencies, as shown in Fig. 14. The CA is biased in Class-AB with of  $V_{\rm GS,CA}$  around -2.8 V and  $V_{\rm DS,CA}$  around 12 V (tuning range from 10 to 14 V ensuring



20-mil Thick Rogers Duroid-5880; ε,:2.2

Fig. 13. Fabricated PD-LMBA prototype.

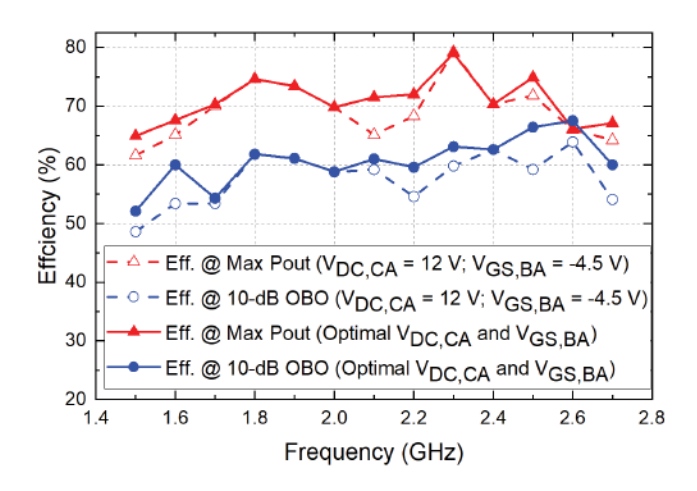


Fig. 14. Simulated power efficiency comparison between consistent  $V_{\rm GS,BA}$ ,  $V_{\rm DS,CA}$ , and optimal  $V_{\rm GS,BA}$  (-5 to -4 V), and  $V_{\rm DS,CA}$  (10-14 V) at  $P_{\rm max}$  and 10-dB OBO levels from 1.5 to 2.7 GHz.

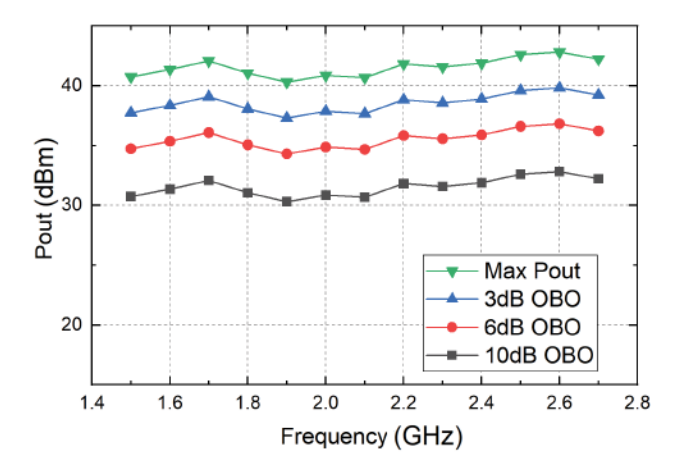


Fig. 15. Measured output power at various OBO levels from 1.5 to 2.7 GHz.

CA saturation at 10-dB OBO). Due to the reduced CA bias voltage and the high-breakdown voltage of GaN transistor, the overdriving of CA does not affect the circuit reliability. In the experiment, the developed PD-LMBA can be well sustainable over prolonged high-power operation. In addition, if the PD-LMBA can be implemented on-chip, the overdriving effect can be mitigated through analog control.

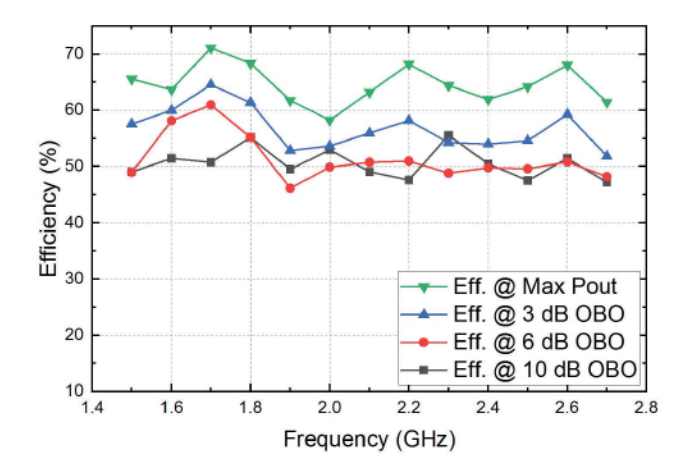


Fig. 16. Measured power efficiency at various OBO levels from 1.5 to 2.7 GHz.

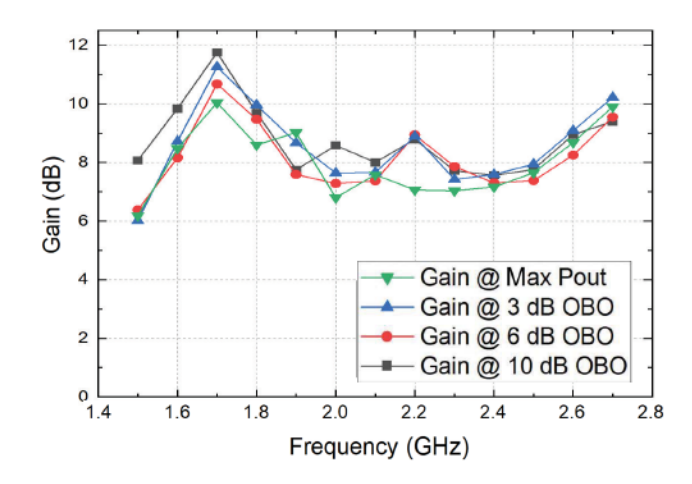


Fig. 17. Measured gain at various OBO levels from 1.5 to 2.7 GHz.

# A. Continuous-Wave Measurement

The prototype is measured under the excitation of a single-tone CW signal from 1.5 to 2.7 GHz at different OBO levels. Fig. 15 shows the maximum output power constantly above 41 dBm over the entire bandwidth. In Fig. 16, the efficiency at maximum power has a local maximum of 72% at 1.7 GHz, and it remains higher than 58% throughout the entire frequency range. The efficiencies at 6- and 10-dB OBO are in the range of 48%–61% and 47%–58%, respectively. The efficiencies here are defined as the ratio between the output power and the total dc power applied to all three amplifiers (i.e., BA1, BA2, and CA), as shown in the following:

Efficiency = 
$$\frac{P_{\text{out}}}{P_{\text{DC,BA1}} + P_{\text{DC,BA2}} + P_{\text{DC,CA}}}.$$
 (10)

It can be seen from Fig. 17 that the gain is maintained around 8 dB. It should be noted that the primary purpose of this article is to demonstrate the proposed concept, and the presented prototype is a first-pass design. Realistically, the gain degradation at band edge and gain fluctuation over frequency can be mitigated with more design iterations. Moreover, the PD-LMBA prototype is measured with

Ref. / Year	Architecture	Freq. (GHz)	FBW (%)	$P_{\mathrm{Max}}$ (dBm)	DE @ $P_{\mathrm{Max}}$ (%)	DE @ HBO (%)	DE @ LBO (%)
[49] 2018	3-Way DPA	0.6-0.9	40	46.1-46.9	51.1-78	51.9-66.2@6 dB	42-64@9.5 dB*
[21] 2018	3-Way DPA	2.0-2.6	26	43.6-45.4	53-76	45-55@6 dB	41-48@8 dB
[22] 2019	3-Way DPA	1.6-2.6	48	45.5-46	53-66	52-66@6 dB	50-53@9.5 dB
[40] 2016	DPA	1.6-2.2	31.6	46-47	60-71	50-55@6 dB*	51-55@10 dB
[50] 2018	DPA	1.5-3.8	86.8	42.3-43.4	42-63	33-55@6 dB	22-40@10 dB*
[20] 2019	DEPA	2.55-3.8	40	48.8-49.8	54-67	42-53@6 dB*	47-60@8 dB
[41] 2017	Dual-Input LMBA	4.5-7.5	50	39	47-77*	28-60@6 dB*	40-72@10 dB* <sup>‡</sup>
[42] 2018	Dual-Input LMBA	1.7-2.5	38	48-48.9	48-58*	43-53@6 dB*	33-45@10 dB*†
[24] 2017	RF-Input LMBA	0.7-0.85	19	42	57-70	34-48@6 dB	30-35@10 dB* <sup>†</sup>
[29] 2017	RF-Input LMBA	1.8-3.8	71	44	46-70	33-59@6 dB	20-25@10 dB* <sup>†</sup>
This Work	PD-LMBA	1.5-2.7	57	43	58-72	47-61@6 dB	47-58@10 dB

TABLE I
STATE OF THE ART OF WIDEBAND LOAD-MODULATED PAS

<sup>\*</sup> Graphically estimated, † PAE, ‡ with reduced  $V_{\rm DD}$ .

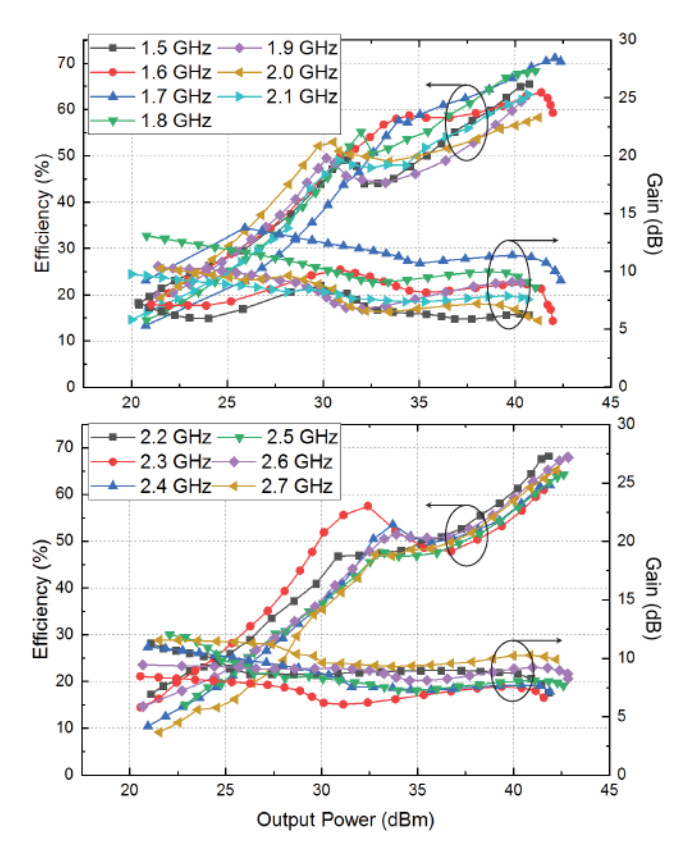


Fig. 18. Power-swept measurement of efficiency and gain from 1.5 to 2.7 GHz.

a power-swept stimulus, and the measured efficiency and gain profiles are plotted in Fig. 18. The shape of the efficiency versus output power curve in Fig. 18 shows a distinct Doherty-like behavior of the PA, which is demonstrated over 10-dB power back-off range at almost every single sample frequency point from 1.5 to 2.7 GHz. These measurement results well validate the proposed PD-LMBA concept and demonstrate the advantage of this new technology in PA efficiency enhancement over a wide bandwidth. The results also indicate that the PD-LMBA is relieved from the original LMBA's [23] reliance on dynamic phase adjustment at a single frequency.

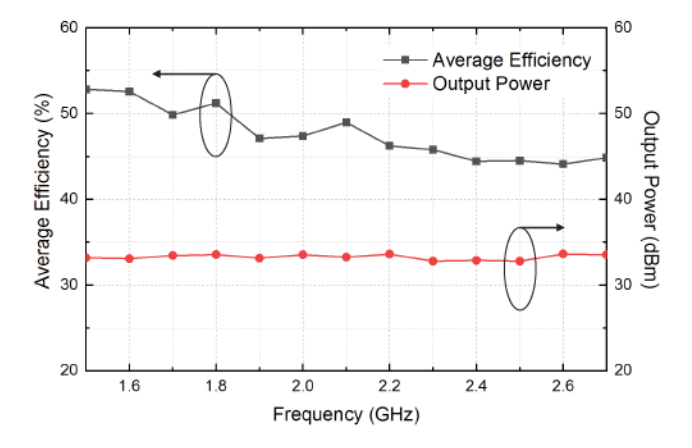


Fig. 19. Measured output power and average efficiency with 9.5-dB-PAPR LTE signal from 1.5 to 2.7 GHz.

Table I presents a comparison between this design and other recently published active-load-modulation PAs with a similar frequency range, output power level, and technology. Even though there is a certain discrepancy between the measurement (see Fig. 18) and the simulation (see Fig. 10), where the measured efficiency drops in the upper power regime at some frequencies, the measured efficiencies (at both  $P_{\rm Max.}$  and various back-off levels) over a broad bandwidth still compare favorably to the state of the art.

#### B. Modulated Measurement

To validate the operation of the designed PD-LMBA in realistic communications, a 10-MHz long term evolution (LTE) signal with a PAPR of 9.5 dB was employed as the stimulation. The modulated signal is generated and analyzed by a Keysight PXIe vector transceiver (VXT M9421). The generated LTE signal is further boosted by a preamplifier (ZHL-5W-422+) to a sufficient level for driving the PD-LMBA. The measurement results at an average output power around 33.5 dBm are presented in Fig. 19. The PD-LMBA achieves a high average efficiency of 47%–58% over the target frequency band. The measured output power spectral density (PSD) is shown

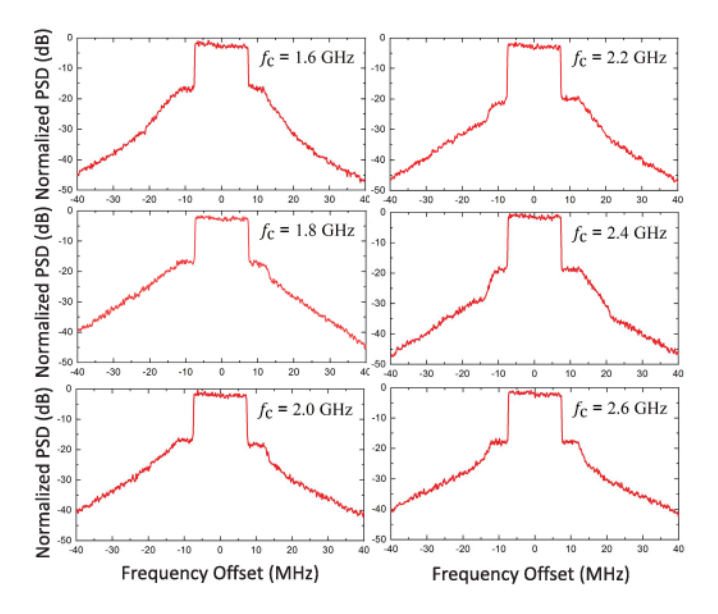


Fig. 20. Output spectrum from modulated measurement using a 10-MHz 9.5-dB-PAPR LTE signal centered at 1.6, 1.8, 2.0, 2.2, 2.4, and 2.6 GHz.

in Fig. 20. The best-case ACLR of 25.8 dB is measured without any digital predistortion.

### VI. CONCLUSION

This article introduces a new type of LMBA with pseudo-Doherty load-modulation behavior. Based on a special combination of CA (carrier) and BA (peaking), this PD-LMBA architecture, for the first time, results in decoupled cooperation of carrier and peaking amplifiers, thus fundamentally eliminating the bandwidth limitation imposed on classic active load-modulation techniques. With proper phase and amplitude controls, an optimal load-modulation behavior can be achieved for PD-LMBA, leading to maximized efficiency over extended power back-off range. More importantly, the efficiency optimization can be achieved with only a static setting of phase offset at a given frequency, which greatly simplifies the complexity for phase control. The measurement results using CW and modulated stimulus signals perfectly validate the proposed PD-LMBA theory and experimentally present a breakthrough on the broadband load-modulated PA in terms of efficiency, back-off range, and bandwidth. Thus, the proposed design method can be considered as a new design paradigm for active load modulation.

### REFERENCES

- M. S. Afaqui, E. Garcia-Villegas, and E. Lopez-Aguilera, "IEEE 802.11ax: Challenges and requirements for future high efficiency Wi-Fi," IEEE Wireless Commun., vol. 24, no. 3, pp. 130–137, Jun. 2017.
- [2] B. Liu, M. Mao, C. C. Boon, P. Choi, D. Khanna, and E. A. Fitzgerald, "A fully integrated class-J GaN MMIC power amplifier for 5-GHz WLAN 802.11ax application," *IEEE Microw. Wireless Compon. Lett.*, vol. 28, no. 5, pp. 434–436, May 2018.
- [3] R. Wu, Y.-T. Liu, J. Lopez, C. Schecht, Y. Li, and D. Y. C. Lie, "High-efficiency silicon-based envelope-tracking power amplifier design with envelope shaping for broadband wireless applications," *IEEE J. Solid-State Circuits*, vol. 48, no. 9, pp. 2030–2040, Sep. 2013.
- [4] W. H. Doherty, "A new high efficiency power amplifier for modulated waves," *Proc. IRE*, vol. 24, no. 9, pp. 1163–1182, Sep. 1936.

- [5] R. Darraji, D. Bhaskar, T. Sharma, M. Helaoui, P. Mousavi, and F. M. Ghannouchi, "Generalized theory and design methodology of wideband Doherty amplifiers applied to the realization of an octavebandwidth prototype," *IEEE Trans. Microw. Theory Techn.*, vol. 65, no. 8, pp. 3014–3023, Aug. 2017.
- [6] V. Camarchia, M. Pirola, R. Quaglia, S. Jee, Y. Cho, and B. Kim, "The Doherty power amplifier: Review of recent solutions and trends," *IEEE Trans. Microw. Theory Techn.*, vol. 63, no. 2, pp. 559–571, Feb. 2015.
- [7] A. Banerjee, L. Ding, and R. Hezar, "High efficiency multi-mode outphasing RF power amplifier in 45nm CMOS," in *Proc. ESSCIRC Conf.* 41st Eur. Solid-State Circuits Conf. (ESSCIRC), Sep. 2015, pp. 168–171.
- [8] J. Hur et al., "A multilevel Class-D CMOS power amplifier for an outphasing transmitter with a nonisolated power combiner," IEEE Trans. Circuits Syst. II, Exp. Briefs, vol. 63, no. 7, pp. 618–622, Jul. 2016.
- [9] R. A. Beltran, "Broadband outphasing transmitter using Class-E power amplifiers," in *IEEE MTT-S Int. Microw. Symp. Dig.*, Jun. 2019, pp. 67–70.
- [10] S. Chung, P. A. Godoy, T. W. Barton, D. J. Perreault, and J. L. Dawson, "Asymmetric multilevel outphasing transmitter using class-E PAs with discrete pulse width modulation," in *IEEE MTT-S Int. Microw. Symp. Dig.*, May 2010, pp. 264–267.
- [11] K. Chen and D. Peroulis, "Design of adaptive highly efficient GaN power amplifier for octave-bandwidth application and dynamic load modulation," *IEEE Trans. Microw. Theory Techn.*, vol. 60, no. 6, pp. 1829–1839, Jun. 2012.
- [12] C. Sanchez-Perez, M. Ozen, C. M. Andersson, D. Kuylenstierna, N. Rorsman, and C. Fager, "Optimized design of a dual-band power amplifier with SiC varactor-based dynamic load modulation," *IEEE Trans. Microw. Theory Techn.*, vol. 63, no. 8, pp. 2579–2588, Aug. 2015.
- [13] H. M. Nemati, C. Fager, U. Gustavsson, R. Jos, and H. Zirath, "Design of varactor-based tunable matching networks for dynamic load modulation of high power amplifiers," *IEEE Trans. Microw. Theory Techn.*, vol. 57, no. 5, pp. 1110–1118, May 2009.
- [14] H. M. Nemati, H. Cao, B. Almgren, T. Eriksson, and C. Fager, "Design of highly efficient load modulation transmitter for wideband cellular applications," *IEEE Trans. Microw. Theory Techn.*, vol. 58, no. 11, pp. 2820–2828, Nov. 2010.
- [15] C. M. Andersson et al., "Theory and design of class-J power amplifiers with dynamic load modulation," *IEEE Trans. Microw. Theory Techn.*, vol. 60, no. 12, pp. 3778–3786, Dec. 2012.
- [16] H. Jang, P. Roblin, C. Quindroit, Y. Lin, and R. D. Pond, "Asymmetric Doherty power amplifier designed using model-based nonlinear embedding," *IEEE Trans. Microw. Theory Techn.*, vol. 62, no. 12, pp. 3436–3451, Dec. 2014.
- [17] H. Oh et al., "Doherty power amplifier based on the fundamental current ratio for asymmetric cells," *IEEE Trans. Microw. Theory Techn.*, vol. 65, no. 11, pp. 4190–4197, Nov. 2017.
- [18] B. Merrick, J. King, and T. Brazil, "A wideband sequential power amplifier," in *IEEE MTT-S Int. Microw. Symp. Dig.*, Jun. 2014, pp. 1–3.
- [19] P. Saad, R. Hou, R. Hellberg, and B. Berglund, "A 1.8–3.8-GHz power amplifier with 40% efficiency at 8-dB power back-off," *IEEE Trans. Microw. Theory Techn.*, vol. 66, no. 11, pp. 4870–4882, Nov. 2018.
- [20] P. Saad, R. Hou, R. Hellberg, and B. Berglund, "The continuum of load modulation ratio from Doherty to traveling-wave amplifiers," *IEEE Trans. Microw. Theory Techn.*, vol. 67, no. 12, pp. 5101–5113, Dec. 2019.
- [21] S. Chen, W. Wang, K. Xu, and G. Wang, "A reactance compensated three-device Doherty power amplifier for bandwidth and back-off range extension," Wireless Commun. Mobile Comput., vol. 2018, pp. 1–10, May 2018.
- [22] J. Xia, W. Chen, F. Meng, C. Yu, and X. Zhu, "Improved three-stage Doherty amplifier design with impedance compensation in load combiner for broadband applications," *IEEE Trans. Microw. Theory Techn.*, vol. 67, no. 2, pp. 778–786, Feb. 2019.
- [23] D. J. Shepphard, J. Powell, and S. C. Cripps, "An efficient broad-band reconfigurable power amplifier using active load modulation," *IEEE Microw. Wireless Compon. Lett.*, vol. 26, no. 6, pp. 443–445, Jun. 2016.
- [24] P. H. Pednekar and T. W. Barton, "RF-input load modulated balanced amplifier," in *IEEE MTT-S Int. Microw. Symp.*, Jun. 2017, pp. 1730–1733.
- [25] D. Collins, R. Quaglia, J. Powell, and S. Cripps, "Experimental characterization of a load modulated balanced amplifier with simplified input power splitter," in *Proc. Asia–Pacific Microw. Conf. (APMC)*, Nov. 2018, pp. 461–463.

- [26] T. Cappello, P. Pednekar, C. Florian, S. Cripps, Z. Popovic, and T. W. Barton, "Supply- and load-modulated balanced amplifier for efficient broadband 5G base stations," *IEEE Trans. Microw. Theory Techn.*, vol. 67, no. 7, pp. 3122–3133, Jul. 2019.
- [27] H. Jeon et al., "A triple-mode balanced linear CMOS power amplifier using a switched-quadrature coupler," IEEE J. Solid-State Circuits, vol. 47, no. 9, pp. 2019–2032, Sep. 2012.
- [28] T. Cappello, P. H. Pednekar, C. Florian, Z. Popovic, and T. W. Barton, "Supply modulation of a broadband load modulated balanced amplifier," in *IEEE MTT-S Int. Microw. Symp. Dig.*, Jun. 2018, pp. 304–307.
- [29] P. H. Pednekar, E. Berry, and T. W. Barton, "RF-input load modulated balanced amplifier with octave bandwidth," *IEEE Trans. Microw. Theory Techn.*, vol. 65, no. 12, pp. 5181–5191, Dec. 2017.
- [30] P. H. Pednekar, W. Hallberg, C. Fager, and T. W. Barton, "Analysis and design of a Doherty-like RF-input load modulated balanced amplifier," *IEEE Trans. Microw. Theory Techn.*, vol. 66, no. 12, pp. 5322–5335, Dec. 2018.
- [31] Y. Cao, H. Lyu, and K. Chen, "Load modulated balanced amplifier with reconfigurable phase control for extended dynamic range," in *IEEE MTT-S Int. Microw. Symp. Dig.*, Jun. 2019, pp. 1335–1338.
- [32] J. Xia, X. Zhu, L. Zhang, J. Zhai, and Y. Sun, "High-efficiency GaN Doherty power amplifier for 100-MHz LTE-advanced application based on modified load modulation network," *IEEE Trans. Microw. Theory Techn.*, vol. 61, no. 8, pp. 2911–2921, Aug. 2013.
- [33] A. Barakat, M. Thian, V. Fusco, S. Bulja, and L. Guan, "Toward a more generalized Doherty power amplifier design for broadband operation," *IEEE Trans. Microw. Theory Techn.*, vol. 65, no. 3, pp. 846–859, Mar. 2017.
- [34] K. B. Niclas, W. T. Wilser, R. B. Gold, and W. R. Hitchens, "Application of the two-way balanced amplifier concept to wide-band power amplification using GaAs MESFET's," *IEEE Trans. Microw. Theory Techn.*, vol. 28, no. 3, pp. 172–179, Mar. 1980.
- [35] Y. Cao, H. Lyu, and K. Chen, "Wideband Doherty power amplifier in quasi-balanced configuration," in *Proc. IEEE 20th Wireless Microw. Technol. Conf. (WAMICON)*, Apr. 2019, pp. 1–4.
- [36] A. Barthwal, K. Rawat, and S. Koul, "Wideband tri-stage Doherty power amplifier with asymmetric current ratios," in *Proc. IEEE MTT-S Int. Microw. RF Conf. (IMaRC)*, Dec. 2016, pp. 1–4.
- [37] X. A. Nghiem, J. Guan, and R. Negra, "Broadband sequential power amplifier with Doherty-type active load modulation," *IEEE Trans. Microw. Theory Techn.*, vol. 63, no. 9, pp. 2821–2832, Sep. 2015.
- [38] C. E. Weitzel, "RF power amplifiers for wireless communications," in 24th Annu. Tech. Dig. Gallium Arsenide Integr. Circuit (GaAs IC) Symposiu, 2006, pp. 323–326.
- [39] J. Kim, B. Fehri, S. Boumaiza, and J. Wood, "Power efficiency and linearity enhancement using optimized asymmetrical Doherty power amplifiers," *IEEE Trans. Microw. Theory Techn.*, vol. 59, no. 2, pp. 425–434, Feb. 2011.
- [40] J. Xia, M. Yang, and A. Zhu, "Improved Doherty amplifier design with minimum phase delay in output matching network for wideband application," *IEEE Microw. Wireless Compon. Lett.*, vol. 26, no. 11, pp. 915–917. Nov. 2016.
- [41] D. J. Shepphard, J. Powell, and S. C. Cripps, "A broadband reconfigurable load modulated balanced amplifier (LMBA)," in *IEEE MTT-S Int. Microw. Symp. Dig.*, Jun. 2017, pp. 947–949.
- [42] R. Quaglia and S. Cripps, "A load modulated balanced amplifier for telecom applications," *IEEE Trans. Microw. Theory Techn.*, vol. 66, no. 3, pp. 1328–1338, Mar. 2018.
- [43] Innovative Power Products, NY, USA. 90 Degree Hybrid Couplers. Accessed: Sep. 15, 2019. [Online]. Available: https://innovativepp.com/product/ipp-7109/
- [44] M. Muraguchi, T. Yukitake, and Y. Naito, "Optimum design of 3-Db branch-line couplers using microstrip lines," *IEEE Trans. Microw. Theory Techn.*, vol. MTT-31, no. 8, pp. 674–678, Aug. 1983.
- [45] Cree, Inc. Wolfspeed, CA, USA. Gallium Nitride Transistor. Accessed: Mar. 23, 2020. [Online]. Available: https://www.cree.com/RF
- [46] K. Chen and D. Peroulis, "Design of highly efficient broadband class-E power amplifier using synthesized low-pass matching networks," *IEEE Trans. Microw. Theory Techn.*, vol. 59, no. 12, pp. 3162–3173, Dec. 2011.
- [47] K. Chen and D. Peroulis, "Design of broadband highly efficient harmonic-tuned power amplifier using in-band continuous class-F<sup>-1</sup>/F mode transferring," *IEEE Trans. Microw. Theory Techn.*, vol. 60, no. 12, pp. 4107–4116, Dec. 2012.

- [48] P. Saad, C. Fager, H. Cao, H. Zirath, and K. Andersson, "Design of a highly efficient 2–4-GHz octave bandwidth GaN-HEMT power amplifier," *IEEE Trans. Microw. Theory Techn.*, vol. 58, no. 7, pp. 1677–1685, Jul. 2010.
- [49] A. Barthwal, K. Rawat, and S. K. Koul, "A design strategy for bandwidth enhancement in three-stage Doherty power amplifier with extended dynamic range," *IEEE Trans. Microw. Theory Techn.*, vol. 66, no. 2, pp. 1024–1033, Feb. 2018.
- [50] J. J. M. Rubio, V. Camarchia, M. Pirola, and R. Quaglia, "Design of an 87% fractional bandwidth Doherty power amplifier supported by a simplified bandwidth estimation method," *IEEE Trans. Microw. Theory Techn.*, vol. 66, no. 3, pp. 1319–1327, Mar. 2018.



Yuchen Cao (Student Member, IEEE) received the bachelor's degree in engineering from Zhejiang University, Hangzhou, Zhejiang, China, in 2011, and the master's degree from Wichita State University, Wichita, KS, USA, in 2016. He is currently pursuing the Ph.D. degree at the Electrical and Computer Engineering Department, University of Central Florida, Orlando, FL, USA.

His research interests include highly efficient broadband power amplifiers, carrier aggregation, and millimeter-wave circuit design.

Mr. Cao was a recipient of the First Place Award of the Student Design Competition on Carrier Aggregation BAW Quadplexer Module in the IEEE Microwave Theory and Techniques Society (IEEE MTT-S) International Microwave Symposium (IMS) in 2018 and 2019, respectively, the Second Place Award of Student Paper Competition in the IEEE WAMICON 2019, and the Third Place Award of the Student Design Competition on High Efficiency Power Amplifier in the IEEE MTT-S IMS 2019.



Kenle Chen (Member, IEEE) received the bachelor's degree in communication engineering from Xi'an Jiaotong University, Xi'an, Shaanxi, China, in 2005, the master's degree in electronics and information engineering from Peking University, Beijing, China, in 2008, and the Ph.D. degree in electrical engineering from Purdue University, West Lafayette, IN, USA, in 2013.

He has extensive experience in wireless and semiconductor industries. From 2015 to 2017, he worked as a Staff RFIC Engineer with Skyworks Solutions,

Inc., Woburn, MA, USA, where he focused on the development of RF front-end modules for advanced mobile platforms. From 2013 to 2015, he worked as a Principal/Lead RFIC Engineer with innovational startups, where he led the research and development of multiple successful products of CMOS-integrated power amplifiers and front-end solutions for the latest WLAN platforms, such as IEEE802.11ac/ax. He is currently an Assistant Professor with the Department of Electrical and Computer Engineering, University of Central Florida, Orlando, FL, USA. His research interests include energy-efficient, wideband, and ultrahigh-speed RF/millimeter-wave (mm-Wave) circuits, extreme-performance power amplifiers in CMOS and compound semiconductor technologies, reconfigurable RF/mm-Wave electronics, and innovational wireless radio architectures and applications.

Dr. Chen serves as the Chair of the IEEE MTT-S/AP-S Orlando Chapter. He is an Associate Editor of the IEEE TRANSACTIONS ON MICROWAVE THEORY AND TECHNIQUES.